



The Discovery of a Luminous Broad Absorption Line Quasar at a Redshift of 7.02

Feige Wang^{1,2,3}, Jinyi Yang², Xiaohui Fan², Minghao Yue², Xue-Bing Wu^{3,4}, Jan-Torge Schindler², Fuyan Bian⁵, Jiang-Tao Li⁶, Emanuele P. Farina¹, Eduardo Bañados⁷, Frederick B. Davies¹, Roberto Decarli⁸, Richard Green², Linhua Jiang³, Joseph F. Hennawi^{1,9}, Yun-Hsin Huang², Chiara Mazzucchelli⁹, Ian D. McGreer², Bram Venemans⁹, Fabian Walter⁹, and Yuri Beletsky¹⁰

¹ Department of Physics, University of California, Santa Barbara, CA 93106-9530, USA; fgwang@physics.ucsb.edu

² Steward Observatory, University of Arizona, 933 North Cherry Avenue, Tucson, AZ 85721, USA

³ Kavli Institute for Astronomy and Astrophysics, Peking University, Beijing 100871, People's Republic of China

⁴ Department of Astronomy, School of Physics, Peking University, Beijing 100871, People's Republic of China

⁵ European Southern Observatory, Alonso de Córdova 3107, Casilla 19001, Vitacura, Santiago 19, Chile

⁶ Department of Astronomy, University of Michigan, 311 West Hall, 1085 South University Avenue, Ann Arbor, MI 48109-1107, USA

⁷ The Observatories of the Carnegie Institution for Science, 813 Santa Barbara Street, Pasadena, CA 91101, USA

⁸ INAF—Osservatorio di Astrofisica e Scienza dello Spazio, via Gobetti 93/3, I-40129, Bologna, Italy

⁹ Max Planck Institut für Astronomie, Königstuhl 17, D-69117, Heidelberg, Germany

¹⁰ Las Campanas Observatory, Carnegie Institution of Washington, Colina el Pino, Casilla 601, La Serena, Chile

Received 2018 October 19; revised 2018 November 9; accepted 2018 November 14; published 2018 December 5

Abstract

Despite extensive efforts, to date only two quasars have been found at $z > 7$, due to a combination of low spatial density and high contamination from more ubiquitous Galactic cool dwarfs in quasar selection. This limits our current knowledge of the super-massive black hole growth mechanism and reionization history. In this Letter, we report the discovery of a luminous quasar at $z = 7.021$, DELS J003836.10–152723.6 (hereafter J0038–1527), selected using photometric data from Dark Energy Spectroscopic Instrument Legacy Imaging Survey, Pan-STARRS1 (PS1) imaging Survey, as well as *Wide-field Infrared Survey Explore* mid-infrared all-sky survey. With an absolute magnitude of $M_{1450} = -27.1$ and bolometric luminosity of $L_{\text{Bol}} = 5.6 \times 10^{13} L_{\odot}$, J0038–1527 is the most luminous quasar known at $z > 7$. Deep optical to near-infrared spectroscopic observations suggest that J0038–1527 hosts a 1.3 billion solar mass black hole accreting at the Eddington limit, with an Eddington ratio of 1.25 ± 0.19 . The C IV broad emission line of J0038–1527 is blueshifted by more than 3000 km s^{-1} relative to the quasar systemic redshift. More detailed investigations of the high-quality spectra reveal three extremely high-velocity C IV broad absorption lines with velocity from 0.08 to 0.14 times the speed of light and total “balnicity” index of more than 5000 km s^{-1} , suggesting the presence of relativistic outflows. J0038–1527 is the first quasar found at the epoch of reionization with such strong outflows, and therefore provides a unique laboratory to investigate active galactic nuclei feedback on the formation and growth of the most massive galaxies in the early universe.

Key words: cosmology: observations – early universe – galaxies: active – galaxies: high-redshift – quasars: individual (J0038–1527)

1. Introduction

As the most luminous non-transient objects, distant quasars are important tracers to study early structure formation and the history of cosmic reionization. The detections of complete Gunn–Peterson (GP) absorption troughs in $z > 6$ quasars mark the end of the reionization epoch at $z \gtrsim 6$ (e.g., Fan et al. 2006). The Ly α damping wing absorption profile (Miralda-Escudé 1998) probes neutral intergalactic medium (IGM) gas at the epoch of reionization (EOR). Currently, only two luminous $z > 7$ quasars have been reported in the literature (Mortlock et al. 2011; Bañados et al. 2018), both of which exhibit signatures of strong damping wing absorption, suggesting that the universe is significant neutral at $z > 7$ (e.g., Bolton et al. 2011; Greig et al. 2017; Bañados et al. 2018; Davies et al. 2018).

The existence of distant luminous quasars (Mortlock et al. 2011; Bañados et al. 2018) provides evidence of billion solar mass super-massive black holes (SMBHs) already formed in the EOR, which poses crucial constraints on their formation and growth mechanisms. SMBH growth is not an isolated process. It has been found to be tightly linked with the growth of their host galaxies (i.e., the $M_{\text{BH}}-\sigma_*$ relation;

Gebhardt et al. 2000). Feedback by wind or outflow driven by black hole (BH) accretion has been invoked in simulations to explain the observed relation (e.g., King 2003; Di Matteo et al. 2005). Observationally, strong outflows are often studied in the rest-frame ultraviolet (UV) via blueshifted broad absorption lines (BALs; Weymann et al. 1991) or strong blue velocity shifts of broad C IV emission lines in luminous quasars (e.g., Richards et al. 2011). These features appear most often at a moderate velocity of $v < 0.1$ times the speed of light (c), but relativistic BALs at $v \sim 0.1-0.3c$ have been also found in a small number of quasars (e.g., Hamann et al. 2013, 2018; Rogerson et al. 2016). The associated kinetic power of these relativistic outflows is estimated to be high enough to play a key role in the co-evolution of SMBHs and galaxies (e.g., Ciccone et al. 2015; Feruglio et al. 2017), as it inevitably shocks against star formation and provide significant metal enrichment to the interstellar medium (ISM) and IGM (e.g., Chartas et al. 2009; Zubovas & King 2013).

However, to date only two $z > 7$ quasars are known, which limits our understanding of the quasar population and their effects on galaxy formation and metal enrichment in the early

Universe, highlighting the need to expand the sample of $z > 7$ quasars. In Wang et al. (2017), we demonstrated that the combination of the Dark Energy Spectroscopic Instrument (DESI)¹¹ Legacy Imaging Surveys (DELS; Dey et al. 2018) with near-infrared (NIR) surveys like the UKIRT Hemisphere Survey (UHS; Dye et al. 2018), and the *Wide-field Infrared Survey Explore* mid-infrared survey (Wright et al. 2010) allows us to search for the highest redshift quasars over a much larger area than previous studies. Recently, we also updated our selection procedure by including the Pan-STARRS1 (PS1) Survey (Chambers et al. 2016) to improve our selection efficiency (Wang et al. 2018).

Here, we report the discovery of a luminous $z > 7$ BAL quasar, DELS J003836.10–152723.6 (hereafter J0038–1527), from our ongoing distant quasar survey. In Section 2, we present our spectroscopic observations and infrared photometric observations. In Section 3, we describe the luminosity and BH mass measurements. In Section 4, we characterize the strong relativistic outflows detected in this quasar. Finally, in Section 5 we briefly discuss the implications and summarize future investigations on high-redshift quasars. All results below refer to a Λ CDM cosmology model with a Hubble parameter of $H_0 = 70 \text{ km s}^{-1} \text{ Mpc}^{-1}$ and density parameters of $\Omega_m = 0.3$, and $\Omega_\Lambda = 0.7$.

2. Observations and Data Analysis

J0038–1527 was selected as a $z > 6.5$ quasar candidate based on DELS and PS1 photometric data. It is detected in both DELS z -band ($z_{\text{AB}} = 21.65 \pm 0.08$) and PS1 y -band ($y_{\text{AB}} = 20.61 \pm 0.10$), but is undetected in PS1 g , r , i , and z bands. The strong dropout nature makes it a promising high-redshift quasar candidate. J0038–1527 is also detected in AllWISE ($W1_{\text{VEGA}} = 16.80 \pm 0.10$, $W2_{\text{VEGA}} = 16.08 \pm 0.21$) and therefore it is unlikely to be a nearby Galactic cool dwarf with high proper motion. J0038–1527 is one of the brightest candidates in our sample, and thus has high priority when taking spectroscopic follow-up observations. We refer to Wang et al. (2017, 2018) for detailed descriptions of the target selection.

The initial spectroscopic observation was obtained on 2018 January 16 with Multiple Mirror Telescope (MMT)/Red Channel Spectrograph using a 270 mm^{-1} grating and $1''.25$ slit, which provide a spectral resolution of $R \sim 500$. The spectrum shows a clear break at $\sim 9700 \text{ \AA}$, which suggests it is a quasar at $z \sim 7$. Subsequent high signal-to-noise ratio (S/N) spectra taken with the MMT and *Magellan*/LDSS3-C confirm it as a quasar at $z > 7$.

We were allocated Very Large Telescope (VLT)/X-SHOOTER DD time (program ID: 2100.A-5033(A)) and the observations were obtained over four nights between 2018 January and July. The total on-source exposure was 12,000 s. We used $0''.9$ slits in both optical (VIS) and NIR arms, which deliver resolutions of $R \sim 8900$ and $R \sim 5600$ in VIS and NIR arms, respectively. The data were reduced using standard European Southern Observatory (ESO) X-SHOOTER pipeline.

Additional NIR spectroscopy was obtained with Gemini/Gemini Near-InfraRed Spectrograph (GNIRS), with a total exposure time of 4.2 hr (program ID: GN-2018A-FT-114). We used the cross-dispersed mode with a $0''.675$ slit, which provides a resolution of $R \sim 750$ from $\sim 0.9 \mu\text{m}$ to $\sim 2.5 \mu\text{m}$.

The GNIRS data was reduced with the XIDL¹² suite of astronomical routines in the Interactive Data Language (IDL). Finally, we produced the combined spectrum using the X-SHOOTER and GNIRS observations and scaled it to match the photometric data for absolute flux calibration. Then we correct the Galactic extinction using the Cardelli et al. (1989) reddening law and $E(B - V)$ from Schlegel et al. (1998). The final calibrated VIS to NIR spectrum is shown in Figure 1.

In order to constrain the rest-frame UV spectral energy distribution (SED) of J0038–1527, we obtained Y , J , H , and K -band photometry using UKIRT/WFCAM (Project ID: U/17B/D04) on 2018 January 20. The on-source exposures were 12 minutes in the Y , J , and K -bands, and 6 minutes in the H -band. The processed data was kindly provided by M. Irwin using the standard Visible and Infrared Survey Telescope for Astronomy (VISTA)/WFCAM data-flow system (Irwin et al. 2004). The photometric properties and derived parameters of J0038–1527 are listed in Table 1.

3. Luminosity and BH Mass

We fit the final calibrated spectrum following the approach detailed in Wang et al. (2015). Briefly, we shift the spectrum to rest frame using an initial redshift, and fit a pseudo-continuum model that includes a power-law continuum, Fe II emission (Vestergaard & Wilkes 2001; Tsuzuki et al. 2006), and Balmer continuum (e.g., De Rosa et al. 2014) to the line-free regions using a $1/\sigma^2$ weighting χ^2 fitting technique. We then fit the Mg II emission and derive the quasar systemic redshift by correcting Mg II redshift to [O III] redshift based on the velocity offset between these two lines of the SDSS quasar composite (Vanden Berk et al. 2001). We iterated this procedure until the difference of input redshift and output redshift is smaller than the uncertainty. Then the spectrum is de-redshifted using the final systemic redshift, which is $z = 7.021 \pm 0.005$. The final fitting yields a power-law continuum of $f_\lambda \propto \lambda^{-1.54 \pm 0.05}$. We measure the rest frame 3000 \AA power-law luminosity to be $\lambda L_{3000 \text{ \AA}} = 4.19 \times 10^{46} \text{ erg s}^{-1}$, and the rest-frame 1450 \AA magnitude to be $m_{1450,AB} = 19.84 \pm 0.08$ and $M_{1450,AB} = -27.10 \pm 0.08$. J0038–1527 is about a half magnitude brighter than the other two known $z > 7$ quasars and is the only known quasar at $z > 6.6$ with $M_{1450,AB} < -27$ (Figure 2). By assuming an empirical conversion factor from the luminosity at 3000 \AA (e.g., Shen et al. 2011), we estimate the bolometric luminosity of J0038–1527 as $L_{\text{bol}} = 5.15 \times \lambda L_{3000 \text{ \AA}} = 2.16 \times 10^{47} \text{ erg s}^{-1} = 5.6 \times 10^{13} L_\odot$.

After subtracting the best-fit pseudo-continuum from the spectrum, we fit Mg II and C IV broad emission lines with two Gaussian profiles for each line. We measure a FWHM of $2994 \pm 140 \text{ km s}^{-1}$ and $8728 \pm 452 \text{ km s}^{-1}$ for Mg II and C IV, respectively. The continuum and line fitting are shown in Figure 1. After applying a virial BH mass estimator (Vestergaard & Osmer 2009) based on the Mg II line, we estimate the SMBH mass of J0038–1527 to be $(1.33 \pm 0.25) \times 10^9 M_\odot$. The accretion rate of this quasar is consistent with Eddington accretion, with an Eddington ratio of $L_{\text{bol}}/L_{\text{Edd}} = 1.25 \pm 0.19$. Note that the Eddington ratio quoted here depends on the virial BH mass estimator that we adopt. Using the relation from McLure & Dunlop (2004), we get an SMBH of $(1.21 \pm 0.36) \times 10^9 M_\odot$ and $L_{\text{bol}}/L_{\text{Edd}} = 1.37$. The quoted uncertainty does not include the

¹¹ <http://desi.lbl.gov/>

¹² <https://github.com/profxj/xidl>

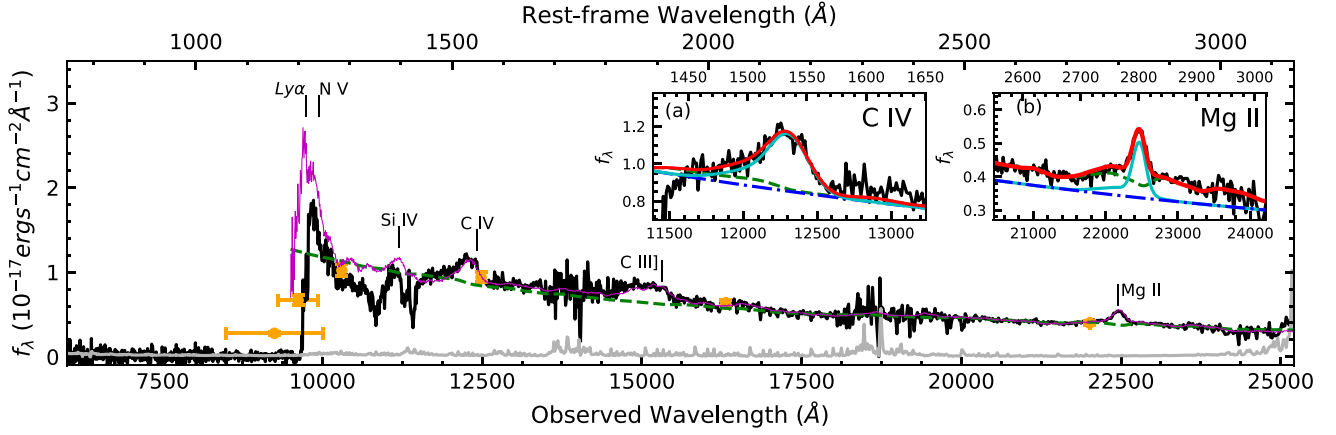


Figure 1. Final calibrated spectrum of J0038–1527. The black and gray lines represent the Galactic extinction corrected spectrum and error vector. The thin magenta line denotes the quasar composite spectrum constructed with ~ 200 Sloan Digital Sky Survey (SDSS) quasars with large C IV blueshifts. The green dashed line denotes the pseudo-continuum, which includes power-law, Fe II emission, and Balmer continuum. The orange circles are flux-density converted from galactic extinction corrected magnitudes listed in Table 1. The x -axis error bars of the two leftmost orange circles denote the FWHMs of z_{DELS} and y_{ps1} filter curves. Two inner plots show spectral fitting of C IV (a) and Mg II (b) regions, respectively. The blue dotted-dashed line denotes the best-fit power-law continuum, the green dashed line denotes the best-fit pseudo-continuum. The cyan line denotes fitted C IV and Mg II emission lines plus power-law continuum, and the red line denotes the total fitted flux.

Table 1
Photometric Properties and Derived Parameters of J0038–1527

R.A. (J2000)	00:38:36.10
Decl. (J2000)	−15:27:23.6
Redshift	7.021 ± 0.005
m_{1450}	19.84 ± 0.08
M_{1450}	-27.10 ± 0.08
$z_{\text{DELS, AB}}$	21.65 ± 0.08
$y_{\text{ps1, AB}}$	20.61 ± 0.10
Y_{VEGA}	19.39 ± 0.08
J_{VEGA}	18.75 ± 0.07
H_{VEGA}	18.15 ± 0.06
K_{VEGA}	17.48 ± 0.05
$W1_{\text{VEGA}}$	16.80 ± 0.10
$W2_{\text{VEGA}}$	16.08 ± 0.21
$g_{\text{ps1}}, r_{\text{ps1}}, i_{\text{ps1}}, z_{\text{ps1}}^a$	$>24.1, 24.0, 23.7, 22.9$
$z_{\text{Mg II}}$	7.025 ± 0.005
$z_{\text{C IV}}$	6.939 ± 0.008
α_{λ}	-1.54 ± 0.05
$\Delta_{\nu\text{C IV}-\nu\text{Mg II}}$ (km s $^{-1}$)	3400 ± 411
$\text{FWHM}_{\text{Mg II}}$ (km s $^{-1}$)	2994 ± 140
$\text{EW}_{\text{Mg II}}$ (Å)	16.5 ± 1.0
$\text{FWHM}_{\text{C IV}}$ (km s $^{-1}$)	8728 ± 452
$\text{EW}_{\text{C IV}}$ (Å)	18.1 ± 1.4
$\lambda L_{3000 \text{ \AA}}$ (erg s $^{-1}$)	4.19×10^{46}
L_{Bol} (erg s $^{-1}$)	2.16×10^{47}
$M_{\text{BH}} (M_{\odot})$	$(1.33 \pm 0.25) \times 10^9$
$L_{\text{Bol}}/L_{\text{Edd}}$	1.25 ± 0.19

Note.

^a Magnitude limits at 3- σ level.

systematic uncertainties in the scaling relation, which could be up to ~ 0.4 dex (Shen et al. 2011).

The BH growth in the early universe is limited by the available accretion time. The existence of J0038–1527 and the other two $z > 7$ quasars requires either massive seed BHs or episodes of super-Eddington accretion under a typical radiation efficiency of $\epsilon \sim 0.1$ to form billion solar mass BHs in a young

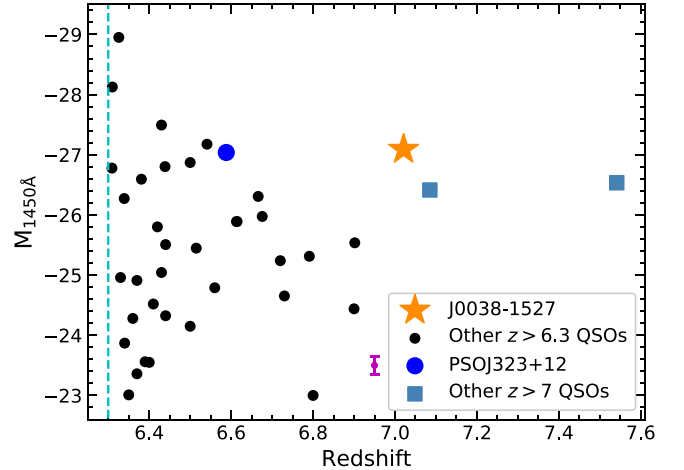


Figure 2. Absolute magnitude of all publicly known $z > 6.3$ quasars. J0038–1527, with $M_{1450,AB} = -27.10$, is the most luminous $z > 6.6$ quasar known to date. The next-highest redshift quasar (PSO323+12 at $z = 6.588$) with comparable luminosity is highlighted by a large blue circle. Two previously known $z > 7$ quasars are denoted by squares. The magenta error bar shows the typical errors on $M_{1450,AB}$ of publicly known quasars. The cyan dashed line mark the position of $z = 6.3$.

Universe. Otherwise, the radiation efficiency must be much lower than that allowed for thin disk accretion.

4. Quasar Outflows

As described in Section 1, quasar outflows are thought to play an important role in regulating the co-evolution of central SMBHs and host galaxies. Both broad emission lines like C IV and highly ionized absorption lines can be efficient diagnostics of quasar outflows. Especially, high-ionization broad emission lines like C IV of quasars are usually blueshifted from the systemic velocity by several hundred km s $^{-1}$ and up to ~ 7000 km s $^{-1}$, depending on the equivalent width (EW) of C IV and the quasar luminosity (e.g., Richards et al. 2011, see also Figure 3). The anti-correlation between continuum luminosity and emission line EW is well known as the Baldwin Effect (Baldwin 1977). More recently, results from the SDSS quasar reverberation mapping

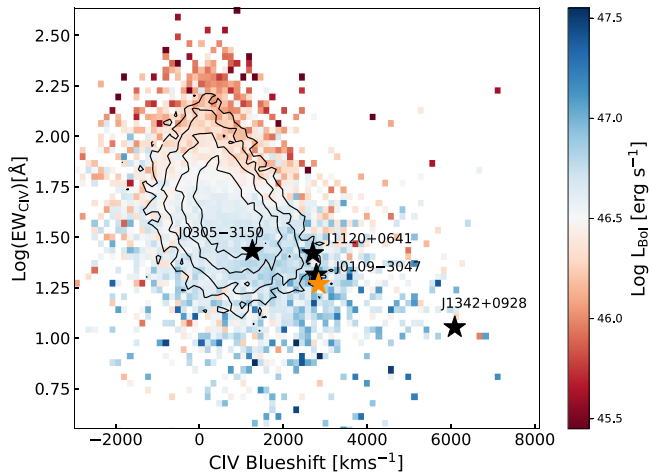


Figure 3. C IV emission line blueshift vs. C IV EW and quasar bolometric luminosity. The contours and 2D histogram are for SDSS low-redshift quasars (Shen et al. 2011) and the black asterisks denote public known $z \gtrsim 6.5$ quasars with C IV observations (e.g., Mortlock et al. 2011; De Rosa et al. 2014; Mazzucchelli et al. 2017; Bañados et al. 2018). The orange asterisk represents J0038–1527. Although all $z \gtrsim 6.5$ quasars are in the large C IV blueshift tail, they are still consistent with the distribution of low-redshift quasars of similarly high luminosities.

project (Sun et al. 2018) show that extreme blueshift quasars have a low level of variability, suggesting that high-blueshift sources tend to also have high Eddington ratios. From our analysis of J0038–1527, we find that the peak of the C IV emission has a strong blueshift with velocity of $3400 \pm 411 \text{ km s}^{-1}$ compared to Mg II. We measured the rest-frame EWs to be $EW_{\text{C IV}} = 18.1 \pm 1.4 \text{ \AA}$ and $EW_{\text{Mg II}} = 16.5 \pm 1.0 \text{ \AA}$. This places J0038–1527 at the high-blueshift velocity end of C IV emission line. In order to further confirm this, we used a more robust way to measure the C IV blueshift explored by Coatman et al. (2016, 2017), which measures the line centroid as the wavelength that bisects the cumulative line flux. This method yields a C IV blueshift of 3800 km s^{-1} , confirms the strong blueshifted C IV emission line in J0038–1527.

More interestingly, after examining the spectrum of J0038–1527, we find several strong BAL features blueward of the C IV and Si IV emission lines. No absorption feature is found blueward of Mg II, indicating that it is a high-ionization broad absorption line quasar (HiBAL). In order to estimate the intrinsic spectrum of J0038–1527, we construct a quasar composite spectrum (Figure 1) using ~ 200 SDSS quasars with extreme C IV emission line blueshifts ($>3300 \text{ km s}^{-1}$). We then divide the spectrum of J0038–1527 by the matched composite to derive a normalized spectrum. From the normalized spectrum, we identified three C IV absorption troughs at extremely high velocities of $(0.14^{+0.03}_{-0.02})c$ (trough A), $(0.10^{+0.005}_{-0.01})c$ (trough B), and $(0.08^{+0.008}_{-0.005})c$ (trough C), which are highlighted with blue, orange, and magenta shaded regions in Figure 4. These three troughs also have accompanied Si IV troughs (top panel in Figure 4). In order to quantify the strength of these troughs, we measure the “balnicity” index (BI; Weymann et al. 1991) of C IV BALs by

$$\text{BI} = \int_{v_{\min}}^{v_{\max}} \left(1 - \frac{f(v)}{0.9}\right) C dv. \quad (1)$$

where $f(v)$ is normalized spectrum, C is set to 1 only when $f(v)$ is continuously smaller than 0.9 for more than 2000 km s^{-1} , otherwise it is set to 0.0. In order to avoid counting absorptions

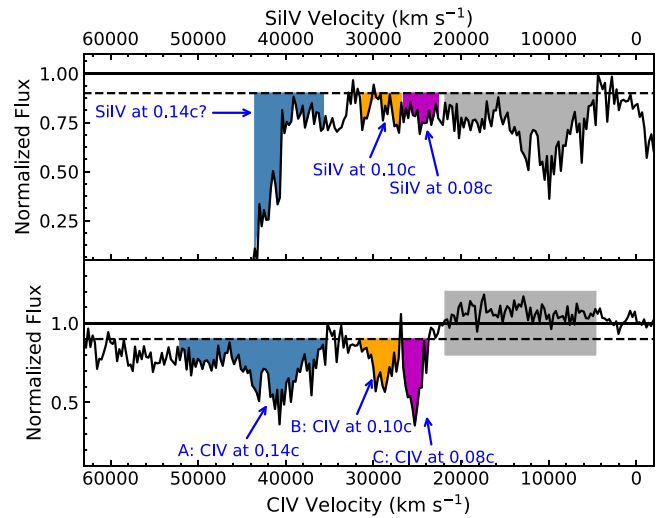


Figure 4. Normalized spectrum of J0038–1527. The x-axis of the top panel is the outflow velocity of Si IV, and the x-axis of the bottom panel shows the outflow velocity relative to C IV. The blue, orange, and magenta shaded regions denote three absorption systems at $0.14c$ (A), $0.10c$ (B), and $0.08c$ (C), respectively. The velocity range of each trough was determined by the C IV trough. The absence of absorption in the gray shaded region in the bottom panel and strong absorption on top of Ly α and N V (blue shaded region in the top panel) suggests that the trough A is indeed an extremely high velocity C IV BAL.

from Si IV, we set $v_{\max} = 52,340 \text{ km s}^{-1}$. The v_{\min} is set to 0. The BIs are measured to be 3400 km s^{-1} , 890 km s^{-1} , and 1010 km s^{-1} for trough A, B, and C, respectively. The uncertainties of the BIs are dominated by the limitations of the template matching accuracy. The total C IV BI of J0038–1527 is 5300 km s^{-1} , which is on the high tail ($\sim 10\%$) of the BI distribution of BAL quasars at lower redshifts (e.g., Gibson et al. 2009).

We note that the composite spectrum matches the spectrum of J0038–1527 very well from C IV to Mg II, but slightly underestimates the continuum blueward of C IV broad emission line. Such difference could be caused by the fact that high-redshift quasars tend to have flatter extinction curves than that of low-redshift quasars (e.g., Maiolino et al. 2004; Gallerani et al. 2010). If so, we might slightly underestimate the BIs measured above. Because trough A has a very high velocity, the associated Si IV absorption trough is blueshifted to the Ly α region, where the spectrum is seriously absorbed by the intervening IGM. On the other hand, the best-fit composite template clearly overfits N V and maybe also Ly α , suggesting strong absorptions over this region, which could be due to Si IV BAL at $\sim 0.14c$. The other possibility for trough A is that it could be a Si IV BAL trough at a lower velocity, as this trough is at the blueward of Si IV emission line. However, we do not see any accompanied C IV troughs at the same velocity shifts (gray shaded region in Figure 4). Without associated C IV troughs, the presence of strong absorption on the top of Ly α and N V emission lines, and the existence of the other two high-velocity troughs (B and C), the spectrum of J0038–1527 strongly suggests that trough A is indeed an extremely high-velocity C IV BAL. Allen et al. (2011) found that the BAL quasar fraction increases by a factor of 3.5 from $z \sim 2$ to $z \sim 4$, which indicates that an orientation effect alone is not sufficient to explain the presence of BAL troughs. This, together with the strong BAL absorptions in J0038–1527 and large C IV

blueshifts found in those $z \gtrsim 7$ quasars, suggests that strong outflows are common in the earliest quasars.

5. Discussion and Summary

As described in Section 4, although most $z > 6.5$ quasars show strong C IV emission line blueshifts, they still follow the locus of low-redshift quasars in Figure 3. Moreover, a low-redshift quasar composite constructed using a simple cut of C IV blueshifts matches the spectrum of J0038–1527 very well. This suggests that the property of C IV emission line is very important for damping wing analysis, as the main uncertainty on such analysis comes from how well one can predict the intrinsic spectra of high-redshift quasars.

The relativistic outflows in this quasar are found with extremely high velocities of $0.08c$ – $0.14c$. Such a phenomenon is very rare and only observed in a small number of low-redshift quasars (e.g., Rogerson et al. 2016; Hamann et al. 2018). Very recently, Hamann et al. (2018) found that highly ionized X-ray ultra-fast outflow (UFO; Chartas et al. 2002; Reeves et al. 2003) in a low-redshift quasar is accompanied with a high-velocity C IV BAL, which suggests that the relativistic C IV BALs might form in the dense clumps embedded in the X-ray UFO. The associated kinetic power of these relativistic outflows is suggested to be well above what is needed to effect quasar host galaxies (e.g., Chartas et al. 2009; Zubovas & King 2013). J0038–1528 is an excellent target to test whether or not AGN feedback could affect the building up progress of massive galaxy with future deep X-ray observations (e.g., Chartas et al. 2009) and (sub-)millimeter observations (e.g., Feruglio et al. 2017). The most distant quasars may have more ubiquitous and stronger outflows of dense gas than their low-redshift counterparts (see also Maiolino et al. 2004). Future larger sample of quasars at $z \gtrsim 7$ are needed to measure the BAL quasar fraction and characterize outflow properties in a statistical manner.

With $M_{1450} = -27.1$, J0038–1527 is the most luminous $z > 7$ quasar known to date. The BH mass of J0038–1527 is measured to be $M_{\text{BH}} = (1.33 \pm 0.25) \times 10^9 M_{\odot}$ based on Mg II emission line. We estimated the bolometric luminosity of J0038–1527 to be $L_{\text{Bol}} = 2.16 \times 10^{47} \text{ erg s}^{-1}$, which yields an Eddington ratio to be $L_{\text{Bol}}/L_{\text{Edd}} = 1.25 \pm 0.19$, suggesting a rapid BH growth phase. The temperature of the accretion disk increases with the accretion rate, and thus produces more UV photons. At the same time, the inner accretion disk is puffed up and could act as a “shielding” gas (e.g., Abramowicz et al. 1988) to block the X-ray emissions. Moreover, the inverse Compton scattering of UV photons cools the hard X-ray corona emission more efficiently resulting in a soft SED (e.g., Jiang et al. 2014a). Quasars with soft SEDs can launch strong winds from the accretion disk (e.g., Jiang et al. 2014b), which could produce the observed strong blueshifts of C IV broad emission lines and BAL features (see Richards et al. 2011, and references therein). Thus, the observed outflows indicated by both C IV emission line blueshifts and BALs are probably driven by high Eddington ratios observed in luminous quasars as suggested by Sun et al. (2018), consistent with the properties observed in J0038–1527.

J. Yang, X. Fan, M. Yue, J.-T. Schindler, and I. D. McGreer acknowledge support from the US NSF grant AST-1515115 and NASA ADAP grant NNX17AF28G. X.-B.W. and L.J. acknowledge support from the National Key R&D Program of

China (2016YFA0400703) and the National Science Foundation of China (11533001 and 11721303). B. Venemans and F. Walter acknowledge funding through the ERC grants “Cosmic Dawn” and “Cosmic Gas.” This research based on observations obtained at the Gemini Observatory (GN-2018A-FT-114) and based on observations collected at the European Organization for Astronomical Research in the Southern Hemisphere under ESO program 2100.A-5033 (A). We especially thank the Directors of VLT, and UKIRT for granting us Director Discretionary time for follow-up observations of this object. We acknowledge the use of data obtained at the Gemini Observatory, Magellan Telescope, and MMT Observatory. We acknowledge the use of public DELS, PS1, and WISE data.

Facilities: Gemini (GNIRS), Magellan (LDSS3-C), MMT (Red Channel Spectrograph), UKIRT (WFCAM), VLT (X-SHOOTER).

ORCID iDs

Feige Wang  <https://orcid.org/0000-0002-7633-431X>
 Jinyi Yang  <https://orcid.org/0000-0001-5287-4242>
 Xiaohui Fan  <https://orcid.org/0000-0003-3310-0131>
 Minghao Yue  <https://orcid.org/0000-0002-5367-8021>
 Xue-Bing Wu  <https://orcid.org/0000-0002-7350-6913>
 Jan-Torge Schindler  <https://orcid.org/0000-0002-4544-8242>
 Fuyan Bian  <https://orcid.org/0000-0002-1620-0897>
 Jiang-Tao Li  <https://orcid.org/0000-0001-6239-3821>
 Emanuele P. Farina  <https://orcid.org/0000-0002-6822-2254>
 Eduardo Bañados  <https://orcid.org/0000-0002-2931-7824>
 Frederick B. Davies  <https://orcid.org/0000-0003-0821-3644>
 Roberto Decarli  <https://orcid.org/0000-0002-2662-8803>
 Linhua Jiang  <https://orcid.org/0000-0003-4176-6486>
 Joseph F. Hennawi  <https://orcid.org/0000-0002-7054-4332>
 Yun-Hsin Huang  <https://orcid.org/0000-0003-4955-5632>
 Chiara Mazzucchelli  <https://orcid.org/0000-0002-5941-5214>
 Ian D. McGreer  <https://orcid.org/0000-0002-3461-5228>
 Bram Venemans  <https://orcid.org/0000-0001-9024-8322>
 Fabian Walter  <https://orcid.org/0000-0003-4793-7880>

References

- Abramowicz, M. A., Czerny, B., Lasota, J. P., & Szuszkiewicz, E. 1988, *ApJ*, 332, 646
- Allen, J. T., Hewett, P. C., Maddox, N., Richards, G. T., & Belokurov, V. 2011, *MNRAS*, 410, 860
- Baldwin, J. A. 1977, *ApJ*, 214, 679
- Bañados, E., Venemans, B. P., Mazzucchelli, C., et al. 2018, *Natur*, 553, 473
- Bolton, J. S., Haehnelt, M. G., Warren, S. J., et al. 2011, *MNRAS*, 416, L70
- Cardelli, J. A., Clayton, G. C., & Mathis, J. S. 1989, *ApJ*, 345, 245
- Chambers, K. C., Magnier, E. A., Metcalfe, N., et al. 2016, arXiv:1612.05560
- Chartas, G., Brandt, W. N., Gallagher, S. C., & Garmire, G. P. 2002, *ApJ*, 579, 169
- Chartas, G., Saez, C., Brandt, W. N., Giustini, M., & Garmire, G. P. 2009, *ApJ*, 706, 644
- Cicone, C., Maiolino, R., Gallerani, S., et al. 2015, *A&A*, 574, A14
- Coatman, L., Hewett, P. C., Banerji, M., et al. 2017, *MNRAS*, 465, 2120
- Coatman, L., Hewett, P. C., Banerji, M., & Richards, G. T. 2016, *MNRAS*, 461, 647
- Davies, F. B., Hennawi, J. F., Bañados, E., et al. 2018, *ApJ*, 864, 142
- De Rosa, G., Venemans, B. P., Decarli, R., et al. 2014, *ApJ*, 790, 145
- Dey, A., Schlegel, D. J., Lang, D., et al. 2018, arXiv:1804.08657
- Di Matteo, T., Springel, V., & Hernquist, L. 2005, *Natur*, 433, 604
- Dye, S., Lawrence, A., Read, M. A., et al. 2018, *MNRAS*, 473, 5113
- Fan, X., Carilli, C. L., & Keating, B. 2006, *ARA&A*, 44, 415
- Feruglio, C., Ferrara, A., Bischetti, M., et al. 2017, *A&A*, 608, A30
- Gallerani, S., Maiolino, R., Juarez, Y., et al. 2010, *A&A*, 523, A85

- Gebhardt, K., Bender, R., Bower, G., et al. 2000, [ApJL](#), **539**, L13
- Gibson, R. R., Jiang, L., Brandt, W. N., et al. 2009, [ApJ](#), **692**, 758
- Greig, B., Mesinger, A., Haiman, Z., & Simcoe, R. A. 2017, [MNRAS](#), **466**, 4239
- Hamann, F., Chartas, G., McGraw, S., et al. 2013, [MNRAS](#), **435**, 133
- Hamann, F., Chartas, G., Reeves, J., & Nardini, E. 2018, [MNRAS](#), **476**, 943
- Irwin, M. J., Lewis, J., Hodgkin, S., et al. 2004, [Proc. SPIE](#), **5493**, 411
- Jiang, Y.-F., Stone, J. M., & Davis, S. W. 2014a, [ApJ](#), **784**, 169
- Jiang, Y.-F., Stone, J. M., & Davis, S. W. 2014b, [ApJ](#), **796**, 106
- King, A. 2003, [ApJL](#), **596**, L27
- Maiolino, R., Oliva, E., Ghinassi, F., et al. 2004, [A&A](#), **420**, 889
- Mazzucchelli, C., Bañados, E., Venemans, B. P., et al. 2017, [ApJ](#), **849**, 91
- McLure, R. J., & Dunlop, J. S. 2004, [MNRAS](#), **352**, 1390
- Miralda-Escudé, J. 1998, [ApJ](#), **501**, 15
- Mortlock, D. J., Warren, S. J., Venemans, B. P., et al. 2011, [Natur](#), **474**, 616
- Reeves, J. N., O'Brien, P. T., & Ward, M. J. 2003, [ApJL](#), **593**, L65
- Richards, G. T., Kruczek, N. E., Gallagher, S. C., et al. 2011, [AJ](#), **141**, 167
- Rogerson, J. A., Hall, P. B., Rodríguez Hidalgo, P., et al. 2016, [MNRAS](#), **457**, 405
- Schlegel, D. J., Finkbeiner, D. P., & Davis, M. 1998, [ApJ](#), **500**, 525
- Shen, Y., Richards, G. T., Strauss, M. A., et al. 2011, [ApJS](#), **194**, 45
- Sun, M., Xue, Y., Richards, G. T., et al. 2018, [ApJ](#), **854**, 128
- Tsuzuki, Y., Kawara, K., Yoshii, Y., et al. 2006, [ApJ](#), **650**, 57
- Vanden Berk, D. E., Richards, G. T., Bauer, A., et al. 2001, [AJ](#), **122**, 549
- Vestergaard, M., & Osmer, P. S. 2009, [ApJ](#), **699**, 800
- Vestergaard, M., & Wilkes, B. J. 2001, [ApJS](#), **134**, 1
- Wang, F., Fan, X., Yang, J., et al. 2017, [ApJ](#), **839**, 27
- Wang, F., Wu, X.-B., Fan, X., et al. 2015, [ApJL](#), **807**, L9
- Wang, F., Yang, J., Fan, X., et al. 2018, [arXiv:1810.11926](#)
- Weymann, R. J., Morris, S. L., Foltz, C. B., & Hewett, P. C. 1991, [ApJ](#), **373**, 23
- Wright, E. L., Eisenhardt, P. R. M., Mainzer, A. K., et al. 2010, [AJ](#), **140**, 1868
- Zubovas, K., & King, A. 2013, [ApJ](#), **769**, 51